RPE | Radiation Physics & Engineering
A Peer-Reviewed Journal
Published by K.N. Toosi University of Technology
http://rpe.kntu.ac.ir
Research Article

Radiation Physics and Engineering 2026; ?(?):?–?

Real-Time radioisotope identification and localization: A scalable and low-cost solution for environmental monitoring

Hadi Ardiny*, Amirmohammad Beigzadeh

Radiation Applications Research School, Nuclear Science and Technology Research Institute, Tehran, Iran

HIGHLIGHTS

-
-
-
-
-

ABSTRACT

To counter the growing threat of illicit radioactive material trafficking, we developed the Radioactive Detection System (RDS), a scalable, low-cost sensor network for real-time radioisotope identification and localization. Each node combines inexpensive detectors (NaI(Tl) scintillation spectrometers or plastic scintillators) with existing surveillance cameras. Machine-vision algorithms fuse radiation measurements with visual tracking to simultaneously quantify intensity and precisely locate moving sources in complex and dynamic urban settings. Laboratory and field tests using concealed sources carried at pedestrian speeds (0.5-1.2 m.s^{-1}) showed: (i) detection and visual localization of a 100 μCi Cs-137 source in 8-25 s; (ii) reliable spectroscopic identification of the Cs-137 within approximately 100 seconds under the reported laboratory testbed configuration. The multi-modal design substantially enhances sensitivity, specificity, and robustness against background fluctuations. With low per-node cost and straightforward integration into existing infrastructure, RDS enables practical large-scale deployment for continuous monitoring of public spaces, critical infrastructure, border checkpoints, and high-security areas, providing an effective tool for radiological threat mitigation.

KEYWORDS
Smart safety
Radiation monitoring
Data fusion
Low-cost
Scalable

HISTORY
Received:
Revised:
Accepted:
Published:

1 Introduction

Radioactive materials are indispensable across medicine, energy, research, and industry. In the medical field, radioactive isotopes are crucial for diagnostic imaging and cancer treatment, significantly improving patient outcomes (Kraft, 2006). Nuclear power plants harness nuclear fission to generate electricity, offering a low-carbon alternative to fossil fuels despite environmental concerns (Adamantiades and Kessides, 2009). Industrial applications utilize radioactive sources for radiography in quality control and fundamental physics research (Johansen and Jackson, 2004). Radioactive sources also find widespread use in fundamental research, enabling crucial processes such as the calibration of particle detectors in high-energy physics experiments, the characterization of material properties through radioactive tracer methods, and the dating of geological and archaeological samples. However, the use of radioactive materials poses significant safety and security risks (Doyle, 2019; Zhu et al., 2024). Unauthorized acquisition, loss, or theft can lead to harmful radiation exposure, environmental contamination, and potential misuse in malicious activities like dirty bombs (Gonzalez, 2001). Mitigating the grave risks associated with radioactive materials requires the development of security protocols and detection systems that are both highly effective and economically viable, enabling widespread deployment to prevent accidents and unauthorized access.

Comprehensive lifecycle management of radioactive materials, from production and use to final waste disposal, is essential for risk reduction (Utami 1997). This

*Corresponding author: hardini@aeoi.org.ir

https://doi.org/

strategy must also be practical and readily implementable. The detection, localization, and identification of radioactive material out of regulatory control (MORC) in real time is a critical challenge for public safety, environmental protection, and national security. Accidental or deliberate releases of radioactive materials can result in severe health risks, economic losses, and social disruption. Traditional radiation detection methods often face significant challenges in terms of scalability, cost-effectiveness, spatial resolution, and sensitivity. These limitations hinder their ability to accurately identify contaminated materials amidst non-contaminated ones, particularly in expansive environments where multiple radiation sources are present. The constraints in scalability make it difficult to deploy these detection systems over large areas efficiently, while the high costs associated with advanced detection technologies limit their widespread adoption. Moreover, the spatial resolution of traditional methods may not be sufficient to pinpoint specific areas of contamination, leading to imprecise detection and potential oversight of hazardous materials. This issue is intensified in large environments with numerous radiation sources. The ability to distinguish between contaminated and non-contaminated materials is crucial for effective radiation management and safety measures. To overcome these challenges, advancements in detection methods are needed, incorporating innovative solutions that enhance scalability, reduce costs, improve spatial resolution, and increase sensitivity. Such improvements would enable more accurate and reliable identification of radioactive materials, ensuring better protection of public health and the environment. Recent advancements in machine vision and data fusion techniques offer new methods for addressing these limitations. Machine vision enables real-time monitoring and tracking of different objects. Furthermore, the integration of diverse detector modalities and imaging systems, each characterized by unique specifications, enables a more comprehensive and accurate characterization of the radiation environment.

This work introduces the Radioactive Detection System (RDS), a low-cost, scalable architecture that resolves directional ambiguity of inexpensive non-directional detectors (NaI(Tl) spectrometers and large-volume plastic scintillators) by fusing their measurements with object trajectories extracted from pre-existing CCTV cameras. Unlike previous multi-modal systems, RDS requires no additional ranging sensors (LiDAR, depth, or stereo) and leverages only ubiquitous surveillance cameras and lightweight computer-vision algorithms, enabling seamless integration into current urban monitoring infrastructure at minimal marginal cost.

The core innovation lies in real-time correlation of time-stamped radiation count rates and energy spectra with visually tracked object positions, allowing simultaneous detection, spectroscopic identification, and precise localization of moving radioactive sources even in the presence of fluctuating natural background.

This study demonstrates the feasibility of the proposed fusion approach in controlled laboratory experiments using concealed Cs-137 (100 μCi) and Co-60 (4.3 μCi) sources carried at pedestrian speeds. We quantify detection times, identification performance, and the influence of detector placement, providing clear evidence that low-cost, camera-enabled scintillation nodes can form the basis of practical, city-scale radiological monitoring networks.

2 Related work

The evolution of radioactive source identification and localization techniques reflects significant advancements in both sensing modalities and deployment strategies. This progression can be categorized into four key phases, each introducing novel approaches to address the limitations of prior methods.

2.1 Static sensor networks and single-modality detection

Early efforts focused on static deployments of radiation detectors, often networked to improve detection reliability. Nemzek et al. pioneered distributed sensing by simulating scintillator networks to track Cs-137 sources, demonstrating enhanced signal-to-noise ratios and localization accuracy compared to individual detectors (Nemzek et al., 2004). Brenann et al. extended this concept using Bayesian methods to characterize detection limits for moving sources, highlighting the trade-offs between sensor density and computational demands (Brennan et al., 2005). Centralized architectures, such as the IoT-integrated system at CERN's REMUS monitoring service, enabled real-time data acquisition and alarm triggering (Manzano et al., 2020). Advanced imaging systems further refined static single-modality approaches. Mihailesco et al. and Vetter et al. developed gamma-ray imaging systems using segmented germanium and Si(Li) detectors, respectively, leveraging Compton scattering and γ-ray tracking to eliminate bulky collimators (Mihailescu et al., 2007; Vetter et al., 2007). Compact designs like the two-sided coded-aperture imager (Ziock et al., 2008) and 1 kg Compton camera (Kataoka et al., 2013) demonstrated portability without sacrificing sensitivity. The High Efficiency Multimode Imager (HEMI) combined Compton and coded-aperture imaging in a static array, enabling spectroscopic characterization (Galloway et al., 2011).

2.2 Multi-modal fusion for enhanced localization

To overcome background interference and directional ambiguity, researchers integrated radiation detectors with complementary sensors. Riley et al. fused unidirectional radiological sensors with 3D depth sensors, resolving directional ambiguities in source tracking (Riley et al., 2015). Another research group describes the Radiological Multisensor Analysis Platform (RadMAP), a mobile detector system designed to study natural gamma-ray and neutron background variations that hinder the detection of weak radiological threats. The authors conducted extensive background measurements and collected contextual

data to test algorithms minimizing false alarms. By integrating gamma-ray and neutron detectors with contextual sensors, RadMAP facilitates data fusion and the creation of detailed multi-sensor datasets, which are used to explore correlations and develop novel detection techniques (Bandstra et al., 2016). Similarly, Cooper et al. detailed the establishment of a city-scale multi-sensor network for the detection and localization of illicit radiological and nuclear materials in urban environments. It highlights the integration of various contextual sensors, including video, Lidar, and meteorological data, to enhance situational awareness and improve detection capabilities (Cooper et al., 2023). Imaging systems also adopted multimodal fusion. A hybrid Compton camera and LiDAR system achieved 3D source mapping in unconstrained environments (Haefner, 2014), while Ardiny et al. presents a novel data fusion and machine vision approach for detecting radiological contamination in moving objects, such as passengers and cars. Utilizing tracking methods to extract features and track objects, the algorithm correlates radiological system data with detected targets (Ardiny et al., 2022). Surveillance systems like the IP camera-NaI(Tl) detector network improved urban monitoring by correlating visual and radiological data (Ardiny and Beigzadeh, 2024). Another study introduced a real-time system that integrates radiological detectors with LiDAR and video tracking to enhance situational awareness and accurately attribute and discriminate radiological sources in complex urban environments (Marshall et al., 2020, 2023).

2.3 Mobile and autonomous deployments

The shift toward mobility addressed the need for rapid, large-area surveillance. UAVs emerged as a critical platform: Pavlovsky et al. introduced the localization and mapping platform (LAMP) for real-time, meter-resolution gamma-ray mapping. Designed for unmanned aerial vehicles (UAVs) and portable use, LAMP efficiently maps large areas while reducing user radiation exposure. It utilizes scene data fusion to integrate radiation and scene data, producing 3D maps of radioactive sources in real time. UAVs equipped with radiation detectors could enhance security by rapidly detecting and localizing orphan source threats. Authors proposed an innovative approach to radiological monitoring by integrating a 2-inch NaI(Tl) detector with a PM tube onto a UAV (Ardiny et al., 2023). Exploration algorithms for effective localization and detection of radioactive hotspots, addressing the limitations of gamma cameras, such as long acquisition times and poor angular resolution investigated by Ardiny et al. They developed behavior-based and multi-criteria decision-making (MCDM) algorithms implemented on an autonomous mobile ground robot (Ardiny et al., 2019). Another research team developed an autonomous mobile robot for localizing unknown radiation sources in a cluttered environment. They employed an information-driven measurement trajectory and utilized a regularized particle filter for continuous parameter estimation (Lazna and Zalud, 2025). Body sensor networks (BSNs) further advanced mobility by relocating sensors dynamically for energy-efficient monitoring.

2.4 Large-scale networks and AI-driven solutions

Recent advancements emphasize scalability and intelligence. IoT enabled AI system designed for the detection and control of nuclear radiation was created by Jacob et al. Utilizing a deep neural network, the system categorizes radiation types and their health impacts, determining safe exposure levels (Jacob et al., 2024). The NYC study showcased a 40,000-detector network using Pearson's Method for data fusion, reducing missed sources by 99% (Flanagan et al., 2024). Visualization tools like the Berkeley data cloud (BDC) facilitated the analysis of large datasets (Weber et al., 2017), while AI-driven algorithms improved threat prioritization and dose estimation (Jacob et al., 2024).

From static networks to AI-enhanced mobile systems, the field has evolved to address challenges in sensitivity, background noise, and operational efficiency. Innovations in multi-modal fusion and autonomous deployment now enable precise, real-time localization in complex environments, laying the groundwork for smart, city-scale nuclear security infrastructures.

2.5 Contributions

Recent advancements in radioactive material detection and localization have focused on optimizing detector technologies (e.g., scintillators, HPGe detectors, Compton cameras) and refining data fusion strategies to address challenges in sensitivity, spatial resolution, and background discrimination. Static sensor networks established the benefits of distributed sensing and Bayesian methods for real-time tracking, while systems like CERN's REMUS and RadMAP integrated contextual sensors to mitigate false alarms. Innovations in imaging, such as compact Compton cameras and hybrid LiDAR-Compton systems, improved directional accuracy, and mobile platforms like UAVs and autonomous robots enabled large-area surveys. Despite these strides, gaps remain in cost-effective scalability, real-time multi-modal fusion, and field readiness for urban deployments. Building on these foundations, this paper introduces a novel system that addresses critical limitations in existing approaches through the following advancements:

- Cost-effective, scalable radioisotope detection: Unlike prior systems reliant on specialized directional sensors (e.g., coded apertures, depth cameras, or 3D-position-sensitive detectors), our design employs ubiquitous surveillance cameras and low-cost radioactive detectors. This eliminates the need for expensive hardware while maintaining compatibility with existing urban infrastructure, offering a scalable solution for widespread deployment.
- Real-time operation for timely response: While earlier frameworks, such as Bayesian networks and IoT architectures, prioritized computational efficiency, our system integrates lightweight machine

vision algorithms to enable real-time processing. This ensures rapid threat identification and decision-making, addressing delays observed in particle-filter-driven robots and computationally intensive fusion methods.

- Enhanced accuracy through multi-modal fusion: Prior multi-modal systems (e.g., RadMAP, LiDAR-Compton hybrids) required complex sensor suites and calibration. By contrast, our approach simplifies fusion by correlating radiation data with camera imagery through lightweight machine vision algorithms, achieving precise source localization without depth sensors or directional detectors. This resolves directional ambiguities inherent in unidirectional systems and outperforms static networks in dynamic environments.

3 Materials and methods

3.1 Experimental setup and testbed

The objective of this study is to identify radioactive sources within a dynamic environment. By integrating data from a camera system and a radiation detector, we developed a method to detect objects emitting ionizing radiation. To validate this approach, experiments were conducted in a controlled laboratory setting, as illustrated in Fig. 1.

Two distinct detector systems were employed in this experiment. The first type, a multi-channel analyzer (MCA) detection system, is situated either at positions A or B, as depicted in Fig. 1. The second type is a single-channel analyzer (SCA) located at position C. To complement these detectors, a 4-megapixel Dh-IPC-HFW1431SP-S4 CCTV camera with 30 frames per second was installed at a height of approximately 2.65 meters adjacent to the MCA node at position A. Figure 2 illustrates the integrated camera and MCA setup. The MCA, a fundamental instrument in nuclear physics for the spectral analysis of ionizing radiation (e.g., gamma and X-rays), employed in this research, integrates a 2-inch NaI(Tl) scintillation crystal coupled to photomultiplier tubes (PMTs) and associated signal processing electronics (amplifier and counter). Incident gamma rays interacting with the scintillator generate scintillation photons, which are detected by the PMT. The PMT's photocathode converts these photons into photoelectrons, subsequently amplified through dynode stages to produce an electrical pulse at the anode, proportional to the deposited energy. The MCA digitizes and bins these pulses according to their amplitude, constructing a radiation energy spectrum. This spectrum enables the identification of radioactive isotopes and the determination of their relative abundances based on their characteristic energy signatures.

Figure 3 illustrates the single-channel analyzer (SCA) detector, a nuclear instrumentation device designed to selectively isolate and count pulses within a user-defined energy window originating from a radiation detector. Pulses meeting this energy criterion are routed to a scaler for event quantification. The SCA utilized in this research incorporates a polyvinyl toluene (PVT) scintillator, a material prevalent in radiation portal monitors owing to its rapid response, high detection efficiency, and cost-effectiveness. Analogous to NaI(Tl) scintillators, PVT emits scintillation photons upon interaction with ionizing radiation. This light is coupled to a photomultiplier tube (PMT), which transduces it into a processable electrical signal for the data acquisition system. PVT scintillators are favored for their robust performance and reliability in radiation detection applications.

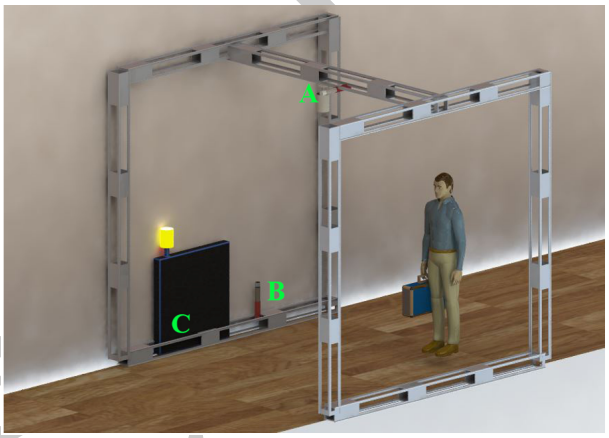

Figure 1: The test-bed considered for the experiment. The MCA node was positioned at location A or B, while the SCA node was placed at location C.

Figure 2: The MCA node and camera were mounted at an elevation of 2.65 meters above the ground; the left image depicts a side view and the right image shows a front view.

Figure 3: The SCA node (plastic scintillator-based) and the MCA node (NaI(Tl) scintillation spectrometer-based) were positioned side-by-side on the testbed.

To validate the spectroscopic performance of the MCA, two standardized radioactive calibration sources, Co-60 and Cs-137, were positioned at a calibrated distance from the detector. The respective activities of these sources were measured as 1.43 and 7.32 mCi. The acquired spectral data, presented in Fig. 4, exhibits distinct photo-peaks corresponding to the characteristic gamma-ray emissions of each isotope: 1173.2 keV and 1332.5 keV for Co-60, and 661.7 keV for Cs-137. The spectra demonstrate the systems energy resolution and its capability to resolve overlapping gamma-ray signatures, confirming the MCA's fidelity in discriminating between isotopes under controlled experimental conditions. The acquired radiation data streams are timestamped and consist of paired gamma-ray counts and corresponding energy channel information for the MCA, and integrated total gamma-ray counts within the defined energy window for the SCA.

3.2 Vision-based object detection and tracking pipeline

Object detection and localization within images are crucial tasks accomplished through various techniques. Traditional tracking algorithms like CSRT and KLT employed in prior studies (Ardiny and Beigzadeh, 2024), and more contemporary AI approaches, such as YOLO (Redmon et al., 2016), are viable options. This experiment involved a suspicious suitcase or package carried on a wheel by an individual, necessitating the application of image processing methods for its detection and localization. The vision subsystem continuously detects the moving target (a suitcase carried by a pedestrian) and estimates its ground-plane position (x, y) in real-world coordinates at 30 Hz. The processing pipeline was intentionally designed to be lightweight, deterministic, and executable on low-power edge hardware typical of existing CCTV deployments. All components were implemented in Python using OpenCV.

Prior to experimentation, the camera was intrinsically and extrinsically calibrated using a 9×6 chessboard captured from multiple viewpoints. OpenCV's 'findChessboardCorners' and 'calibrateCamera' functions were used to obtain intrinsic parameters (focal length, principal point, distortion coefficients) and per-view extrinsic parameters (Fig. 5). Lens distortion was removed in real time using 'undistort()'. A planar 'homography' matrix $H \in R^{3\times3}$ was then estimated with 'findHomography()' from four known floor points in the image and their corresponding metric coordinates. This 'homography' maps any image pixel directly to ground-plane coordinates under the assumption that all objects move on a planar surface, which holds in the laboratory environment.

This figure illustrates the impact of camera calibration. The right image shows the pre-calibration state, where lens distortion is evident in the curvature of the chessboard grid. This distortion is effectively corrected after calibration, which determines both intrinsic and extrinsic camera parameters, as shown in the left image.

Because the experiments involve only a single salient object, complex data-association strategies are unnecessary. Frame-to-frame linkage is performed via nearest-neighbor centroid matching with a maximum gating radius of 100 pixels. If no valid detection is obtained for more than 0.5 s, the track is terminated and re-initialized upon the next detection.

This approach offers several advantages: (i) extremely low computational cost (< 10 % CPU), (ii) no requirement for training data or deep-learning inference, (iii) fully deterministic behavior, and (iv) sub-deci-metre spatial accuracy, which is sufficient for correlation-based source attribution. Its limitations include: (i) strong dependence on color distinctiveness and stable illumination, (ii) susceptibility to partial or full occlusion, and (iii) lack of re-identification following prolonged track loss.

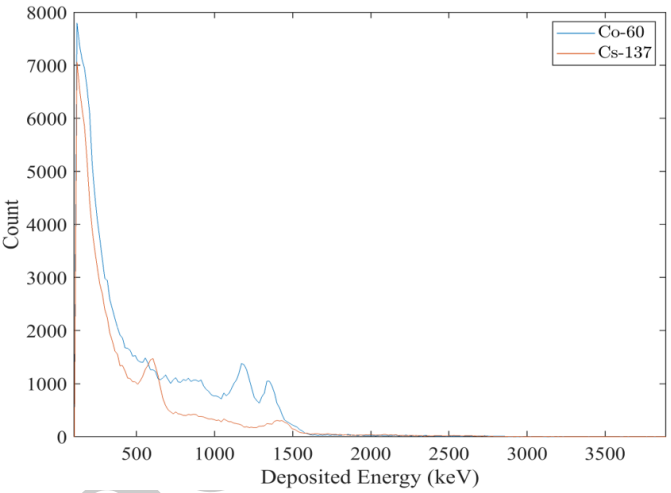

Figure 4: Energy spectra were acquired for Co-60 sources (with an activity of 1.43 mCi) and Cs-137 sources (with an activity of 7.32 mCi) using the MCA.

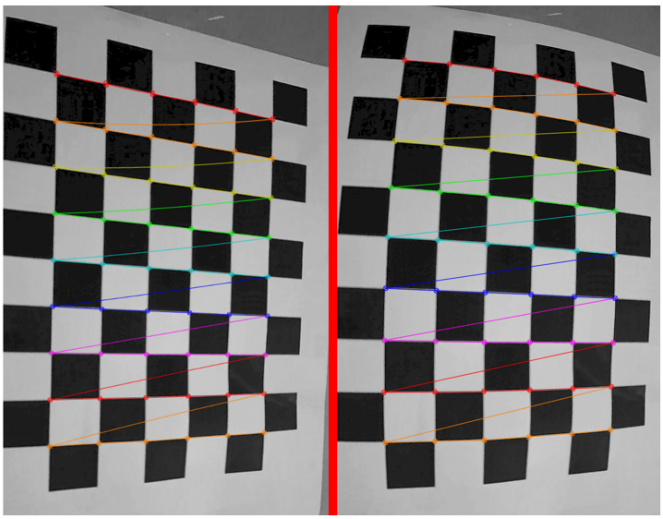

Figure 5: This figure illustrates the impact of camera calibration. The right image shows the pre-calibration state, where lens distortion is evident in the curvature of the chessboard grid. This distortion is effectively corrected after calibration, which determines both intrinsic and extrinsic camera parameters, as shown in the left image.

Figure 6: The color segmentation and detection of luggage were achieved using image processing techniques. The right image displays the original image with the detected object outlined in a red bounding box, while the left image demonstrates the separation of target pixels from the background.

The current color-based tracking pipeline is intentionally optimized for controlled, single-object scenarios such as checkpoint or gate monitoring, where lighting is stable, occlusion is minimal, and only one salient object traverses the field of view at a time. In such settings, the lightweight, deterministic approach offers sufficient accuracy with minimal computational overhead. For wide-area or multi-lane deployments involving multiple moving objects, complex backgrounds, or variable illumination, the vision module can be seamlessly upgraded to a deep-learning tracker (e.g., YOLOv8 + ByteTrack) without modifying the downstream fusion logic-the homography-based projection and correlation-based attribution remain unchanged. This modularity allows RDS to scale from low-cost pilot deployments to complex urban environments while preserving the core fusion architecture.

3.3 Data fusion

The fusion task is to solve for unknown parameters $= A(activity), (x, y, z)(t)(position), E(isotope)$ given three heterogeneous measurements. Individually, each sensor leaves the problem severely under-determined. Together they are over-determined:

- Vision: Achieve high-precision continuous tracking of the (x, y) position over time for every individual object in the field.
- SCA: Rapid scalar count-rate signal $C(t) \propto \sum_j (A_j / r_j^2(t))$ where $C(t)$ is total detected counts.s^{-1}, A_j is activity of source j, and $r_j(t)$ is instantaneous distance from detector to source j.
- MCA mode: Full energy-resolved vector spectrum $S(E, t)$ where the spectrum is isotope-labeled (E axis corresponds to characteristic γ-lines of specific isotopes) and recorded continuously as a function of time t.

Once the luggage is successfully identified and located, the relative distance between the center of the red rectangle encompassing the luggage and the centers of the detectors can be calculated. The object's positions relative to the camera are timestamped and transformed to a fixed reference frame (i.e., the detector's position). Due to disparate acquisition frequencies, with radiation data sampled at 1 Hz and vision-derived positional data at 30 Hz, a 1-second integration window was employed. To synchronize the positional information with the lower-frequency radiation data, an averaging filter was applied to the vision-based position data over this 1-second integration period. As previously documented in existing research (Ardiny and Beigzadeh, 2024; Ardiny et al., 2022), the correlation coefficient between this distance and the detector's recorded radiation count per second (CPS) can serve as an indicator of source presence. The correlation coefficient is a statistical metric that quantifies the relationship and interdependence between two quantitative variables. It reflects both the strength and nature of the relationship, ranging from -1 to 1. A positive correlation coefficient implies that an increase or decrease in one variable corresponds to a similar change in the other. Conversely, a negative correlation indicates an inverse relationship. A correlation coefficient close to or equal to zero suggests a lack of correlation, implying independence between the two variables. The correlation between two random variables, X and Y, is formally defined as follows:

$$correlation(X.Y) = \frac{covariance(X.Y)}{\sigma_X \sigma_Y} \tag{1}$$

where σ is the standard deviation of the data. The primary variables under investigation are the distance from the detector and the corresponding gamma-ray count. An inverse relationship is anticipated between these two variables, such that an increase in distance leads to a decrease in gamma ray count. Consequently, the correlation coefficient between these variables should be a negative value. Conversely, if the moving object lacks a radiation source, variations in distance will not influence the radiation count, resulting in a correlation coefficient closer to zero.

Formally, the output of the RDS is defined as the triplet: binary alarm decision, carrier image, and precise spatiotemporal localization. the stability of the correlation coefficient serves as the primary evaluation criterion. A consistent negative correlation indicates that the vision-derived coordinates (x, y) successfully model the physical relationship between the source and detector, providing a self-consistent validation of the localization accuracy.

4 Results and discussion

The experimental setup, as depicted in Fig. 1, involved a person carrying a suitcase containing a Cs-137 source with an activity of 100 mCi. The individual moved randomly within the laboratory environment. Previous research (Ardiny and Beigzadeh, 2024; Ardiny et al., 2022) has demonstrated that an object carrying the source (contaminated object) exhibits a stable and distinct correlation coefficient beyond a threshold value of approximately -0.4. However, the precise threshold value is influenced by experimental factors such as distance and source strength. Moreover, experimental setup parameters can impact the temporal evolution of the correlation signal, determining the point at which it stabilizes and becomes distinguishable beyond the specified threshold. Therefore, this study aimed to identify contaminated objects through the continuous monitoring of the correlation coefficient between the distance from the object and measured gamma radiation counts. This involved the identification of correlation values indicative of a strong negative relationship and the subsequent demonstration of a temporally stable graphical representation of this correlation, serving as a robust indicator of contamination. In the initial test, the MCA node was positioned at a height of 2.65 meters above the ground position A (Fig. 1). In contrast, the SCA node was placed adjacent to it at position C (Fig. 1). The results of Fig. 7, representing 50 series of count and distance correlation data at 200 seconds, indicate that the contaminated object was not detected at this height. The reduced radiation count at the higher elevation and the proximity of the detector to the noise level hindered the detection of displacement changes, leading to a weak signal. However, the SCA node successfully identified the source within the first 20 seconds. This improved performance can be attributed to its larger volume and closer proximity to the source compared to MCA.

Figure 8 illustrates the temporal evolution of the gamma-ray spectral data acquired by the MCA. Each depicted graph represents a spectrum recorded at 50-second intervals. A trend reveals a gradual increase in the count rate within the Cs-137 energy channel as the acquisition time progresses. Notably, the augmentation in the Cs-137 channel becomes apparent from approximately 100 seconds onward.

In the next experiment, the MCA node was relocated to a position on the wall near the ground surface, designated as position B in Fig. 1. By repositioning the MCA, the contaminated object was accurately identified, as illustrated in Fig. 9. This successful detection demonstrates the MCA's ability to track the random movements of the person within the laboratory environment. The low standard deviation observed in the data further supports this claim, indicating the detector's sensitivity to subtle changes in the person's position. After approximately 30 seconds, the correlation coefficient stabilized at -0.62, representing a strong negative value. This significant drop indicates the successful detection of the contaminated object's location within the first ten seconds. Despite the larger volume of the SCA node, the MCA node exhibited performance in this scenario. Its proximity to the source and the narrower field of view (FOV) contributed to a more precise detection of the source's displacement ratio, resulting in enhanced resolution.

The previous experiment was repeated using a Co-60 radioactive source with an activity of 4.32 mCi. As the graph in Fig. 10 shows, the correlation coefficient of the MCA node could not reach a strong negative value, indicating a weaker correlation between the measured data and the expected pattern. However, the SCA node was able to detect the presence of the Co-60 source. This suggests that SCA node, particularly those with larger sizes, may be more sensitive to detecting very low-activity radioactive sources.

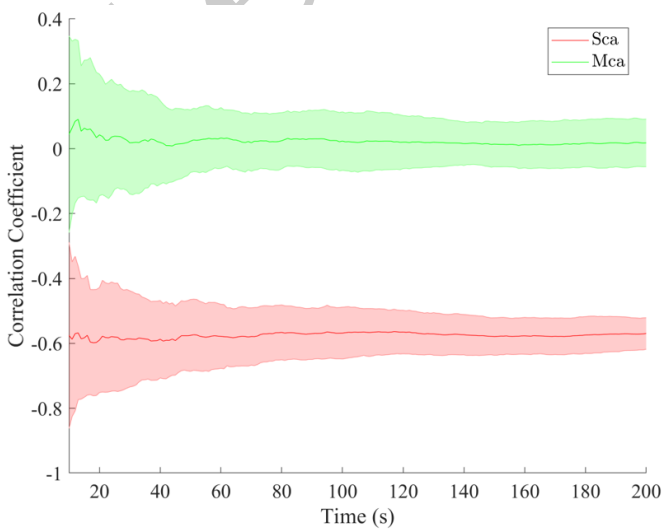

Figure 7: The correlation coefficient was calculated for 50 data series obtained from the MCA node at position A and the SCA node after 200 seconds of operation.

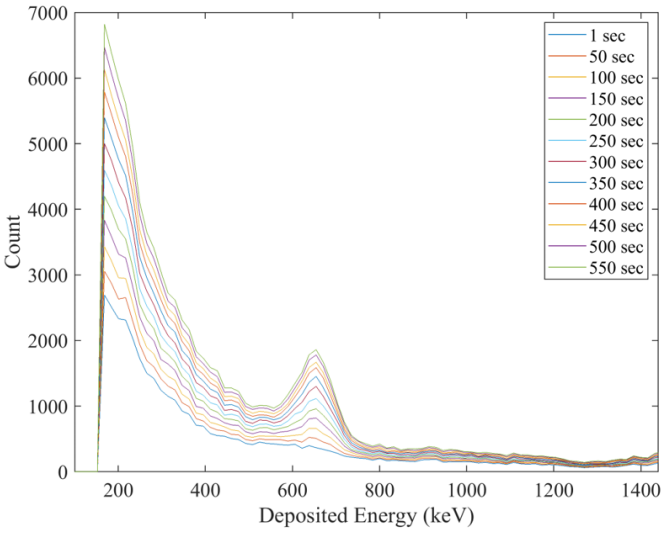

Figure 8: Spectral data acquired via the MCA demonstrated observable growth in the Cs-137 spectral peak, with a statistically increase emerging at 100 seconds

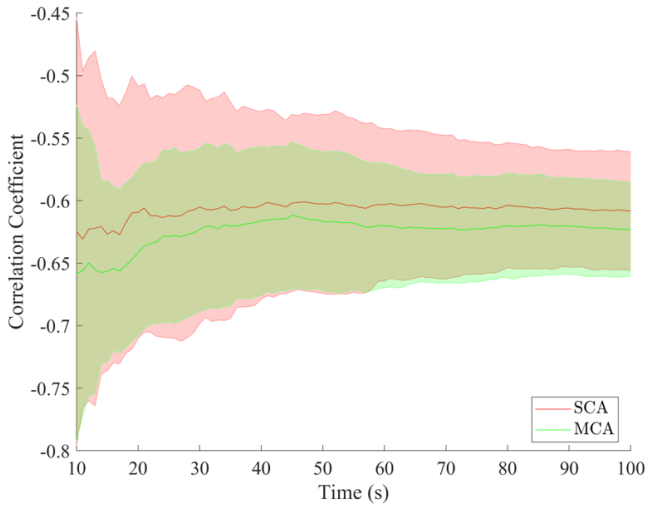

Figure 9: Correlation coefficient for Cs-137 (100 μCi) after 100 seconds across 50 data series for MCA at position B and SCA.

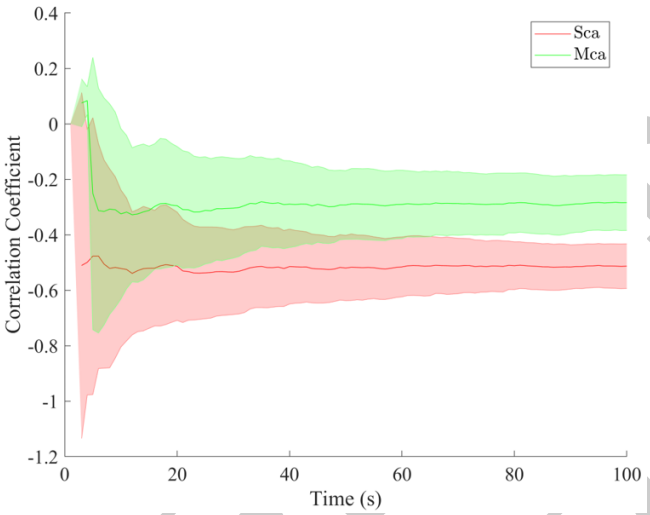

Figure 10: Correlation coefficient for Co-60 (4.32 mCi) after 100 seconds for 50 data series for MCA installed at position B and SCA.

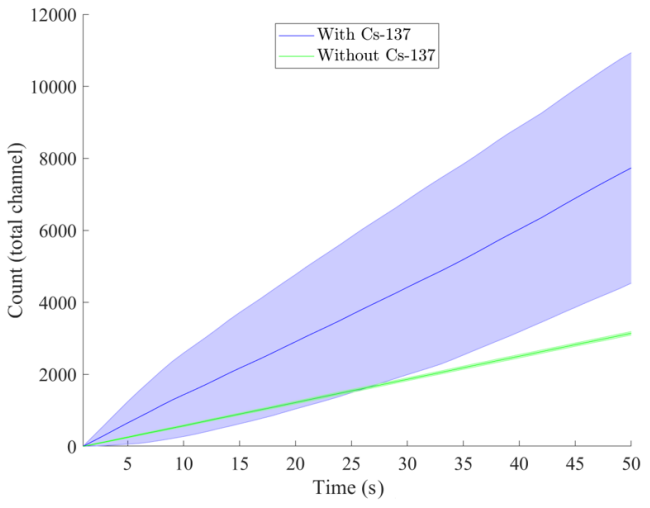

Figure 11: Growth rates of the Cs-137 channel were compared for 50 data series, with and without the presence of a Cs-137 source.

To quantitatively assess the detector's performance in source identification under both background and source-present conditions, the temporal resolution required to achieve accurate classification of the radioactive source type was determined. Focusing on the Cs-137 energy channel at 662 keV, the energy growth of this channel relative to the background was analyzed. The presence of a Cs-137 source significantly influenced the energy growth of the related channel, as illustrated in Fig. 11.

To ensure the correctness of the function and assumption, the channels related to the energy peaks of Co-60 (1173.2 and 1332.5 keV) have also been considered, and the energy growth of this channel has been examined with the background. As Fig. 12 shows, the growth of the Co-60 channel when the Cs-137 source is present is less than the background, which indicates that the Co-60 source channel has a lower growth than the background and the rays emitted in the Cs-137 channel are aggregated.

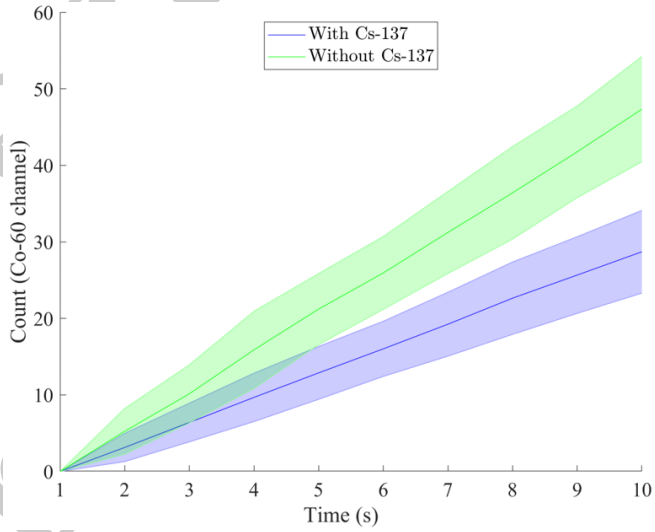

Figure 12: Growth rates of the Co-60 channel were compared for 50 data series, with and without the presence of a Cs-137 source.

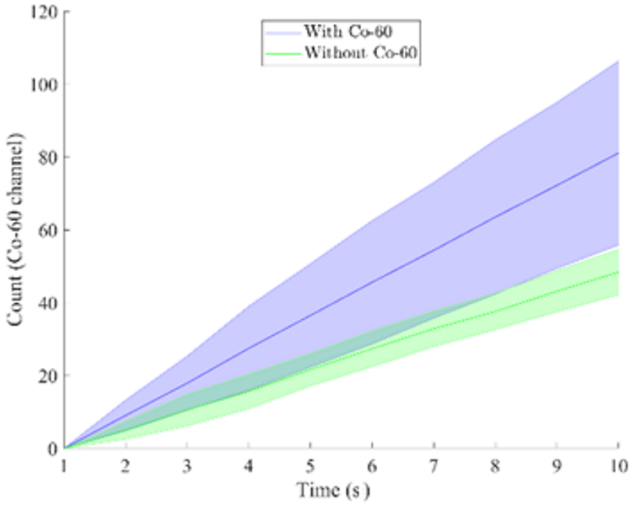

Figure 13: Growth rates of the Cs-60 channel were compared for 50 data series, with and without the presence of a Co-60 source.

To further investigate the behavior of the system, we examined the growth of the Co-60 channel while the Co-60 source was in motion. As illustrated in Fig. 13, the growth of the Co-60 channel in this scenario was also observed to be higher than the background level. This finding reinforces the previous observation that the Co-60 source channel exhibits a slower accumulation rate compared to the background in the presence of the Cs-137 source.

5 Conclusions

The development of an intelligent monitoring system integrating vision and radiation spectroscopy represents a significant advancement in societal safety and security. This system, capable of locating, identifying, and detecting radioactive materials, effectively merges visual data from urban cameras with spectroscopic measurements. This approach allows for accurate detection and positioning of radiation sources in various environments. The integration of these two methods improves the reliability and speed of radioactive material detection and spatial information, which is essential for timely responses to radiation threats or incidents. This capability is invaluable for action groups such as relief and rescue teams, enabling them to make informed decisions and take appropriate actions. Our findings highlight the importance of strategic detector placement. While the presence of radioactive sources at low heights can be addressed by positioning MCAs on walls or floors, detecting contaminated objects may necessitate more powerful detectors or alternative detector placements. While this MCA has limitations in precisely locating and tracking sources with low radioactivity levels, their ability to accumulate gamma-ray spectra over time enables them to detect and identify even low-energy radioactive materials. This is particularly useful for applications requiring the identification of subtle radiation sources.

The potential applications of this technology extend to critical infrastructure protection, environmental monitoring for radioactive contamination, border security, and emergency response. To fully realize its benefits, future research and development must focus on enhancing the system's robustness, scalability, and accuracy. This will ensure comprehensive radiological monitoring and protection, thereby contributing significantly to safety and environmental protection. In our next research endeavor, we aim to address the scalability of this system to facilitate its deployment in real-world urban environments. The current study serves as a fundamental validation of the fusion logic within a single-room, single-object testbed. While the underlying tracking algorithms (e.g., YOLO/ByteTrack) are natively capable of simultaneous multi-object processing, the experimental verification of the system's performance in high-density, multi-source scenarios remains outside the scope of this paper and is designated for future work.

Acknowledgements

Part of the funding for this project was provided through a coordinated research project: "Facilitation of safe and secure trade using nuclear detection technology - detection of RN and other contraband (J02015)".

Conflict of Interest

The authors declare no potential conflict of interest regarding the publication of this work.

References

Adamantiades, A. and Kessides, I. (2009). Nuclear power for sustainable development: current status and future prospects. *Energy Policy*, 37(12):5149–5166.

Ardiny, H. and Beigzadeh, A. (2024). Exploring radiological contamination among the same moving objects based on a fusion between radioactive detectors and surveillance cameras. *The European Physical Journal Plus*, 139(2):172.

Ardiny, H., Beigzadeh, A., and Askari, M. (2022). Detecting and tracking multiple mobile radioactive sources by data fusion of a surveillance camera and a sodium iodide (NaI) detector. *Review of Scientific Instruments*, 93(12).

Ardiny, H., Beigzadeh, A., and Mahani, H. (2023). MCNPX simulation and experimental validation of an unmanned aerial radiological system (UARS) for rapid qualitative identification of weak hotspots. *Journal of Environmental Radioactivity*, 258:107105.

Ardiny, H., Witwicki, S., and Mondada, F. (2019). Autonomous exploration for radioactive hotspots localization taking account of sensor limitations. *Sensors*, 19(2):292.

Bandstra, M. S., Aucott, T. J., Brubaker, E., et al. (2016). Radmap: The radiological multi-sensor analysis platform. *Nuclear Instruments and Methods in Physics Research Section A: Accelerators, Spectrometers, Detectors and Associated Equipment*, 840:59–68.

Brennan, S. M., Mielke, A. M., and Torney, D. C. (2005). Radioactive source detection by sensor networks. *IEEE Transactions on Nuclear Science*, 52(3):813–819.

Cooper, R., Abgrall, N., Aversano, G., et al. (2023). Networked sensing for radiation detection, localization, and tracking. In *Journal of Physics: Conference Series*, volume 2586, page 012125. IOP Publishing.

Doyle, J. E. (2019). Confronting a nuclear north korea. In *Nuclear Safeguards, Security, and Nonproliferation*, pages 137–154. Elsevier.

Flanagan, R., Osborne, A., and Deinert, M. (2024). Data synthesis improves detection of radiation sources in urban environments. *Nuclear Instruments and Methods in Physics Research Section A: Accelerators, Spectrometers, Detectors and Associated Equipment*, 1058:168821.

Galloway, M. L., Amman, M., Awadalla, S., et al. (2011). Status of the high efficiency multimode imager. In *2011 IEEE Nuclear Science Symposium Conference Record*, pages 1290–1293. IEEE.

Gonzalez, A. J. (2001). Security of radioactive sources. The evolving new international dimensions.

Haefner, A. (2014). *Compton Image Reconstruction Algorithms and Demonstration Across Multiple Devices: From the Lab to the Field*. PhD thesis, University of California, Berkeley.

Jacob, N., Orji, C., et al. (2024). Nuclear radiation detection and control system using artificial neural network (ANN) approach. *African Journal of Engineering and Environment Research*, 6:1.

Johansen, G. A. and Jackson, P. (2004). *Radioisotope gauges for industrial process measurements*. Wiley Online Library.

Kataoka, J., Kishimoto, A., Nishiyama, T., et al. (2013). Handy Compton camera using 3D position-sensitive scintillators coupled with large-area monolithic MPPC arrays. *Nuclear Instruments and Methods in Physics Research Section A: Accelerators, Spectrometers, Detectors and Associated Equipment*, 732:403–407.

Kraft, A. (2006). Between medicine and industry: Medical physics and the rise of the radioisotope 1945–65. *Contemporary British History*, 20(1):1–35.

Lazna, T. and Zalud, L. (2025). Localizing multiple radiation sources actively with a particle filter. *Nuclear Engineering and Technology*, 57(2):103171.

Manzano, L. G., Bisegni, C., Boukabache, H., et al. (2020). A distributed and interconnected network of sensors for environmental radiological monitoring. *Radiation Measurements*, 139:106488.

Marshall, M., Cooper, R., Curtis, J., et al. (2023). Mobile object tracking in panoramic video and LiDAR for radiological source-object attribution and improved source detection. *arXiv preprint arXiv:2309.06592*.

Marshall, M., Hellfeld, D., Joshi, T., et al. (2020). 3-d object tracking in panoramic video and lidar for radiological source–object attribution and improved source detection. *IEEE Transactions on Nuclear Science*, 68(2):189–202.

Mihailescu, L., Vetter, K., Burks, M., et al. (2007). SPEIR: a Ge Compton camera. *Nuclear Instruments and Methods in Physics Research Section A: Accelerators, Spectrometers, Detectors and Associated Equipment*, 570(1):89–100.

Nemzek, R. J., Dreicer, J. S., Torney, D. C., et al. (2004). Distributed sensor networks for detection of mobile radioactive sources. *IEEE Transactions on Nuclear Science*, 51(4):1693–1700.

Redmon, J., Divvala, S., Girshick, R., et al. (2016). You only look once: Unified, real-time object detection. In *Proceedings of the IEEE conference on Computer Vision and Pattern Recognition*, pages 779–788.

Riley, P., Enqvist, A., and Koppal, S. J. (2015). Low-cost depth and radiological sensor fusion to detect moving sources. In *2015 International Conference on 3D Vision*, pages 198–205. IEEE.

Vetter, K., Burks, M., Cork, C., et al. (2007). High-sensitivity Compton imaging with position-sensitive Si and Ge detectors. *Nuclear Instruments and Methods in Physics Research Section A: Accelerators, Spectrometers, Detectors and Associated Equipment*, 579(1):363–366.

Weber, G. H., Bandstra, M. S., Chivers, D. H., et al. (2017). Web-based visual data exploration for improved radiological source detection. *Concurrency and Computation: Practice and Experience*, 29(18):e4203.

Zhu, W., Zhao, R., Tang, X., et al. (2024). Evaluation of radiation leakage in X-ray security inspection machine using a CZT spectrometer. *Radiation Measurements*, 177:107274.

Ziock, K.-P., Cunningham, M., and Fabris, L. (2008). Two-sided coded-aperture imaging without a detector plane. In *2008 IEEE Nuclear Science Symposium Conference Record*, pages 634–641. IEEE.

To cite this article:

H. Ardiny, A. Beigzadeh. Real-Time radioisotope identification and localization: A scalable and low-cost solution for environmental monitoring. *Radiation Physics and Engineering*, In Press.

DOI:

To link to this article: